Liquid metal embrittlement of a dual-phase $Al_{0.7}CoCrFeNi$ high-entropy alloy exposed to oxygen-saturated lead-bismuth eutectic

Xing Gong[a,*], Congying Xiang[b], Thierry Auger[c], Jiajun Chen[a], Xiaocong Liang[b], Zhiyang Yu[b,*], Michael P Short[d], Min Song[e], Yuan Yin[a]

[a] *Advanced Nuclear Energy Research Team, College of Physics and Optoelectronic Engineering, Shenzhen University, Shenzhen 518060, China*
[b] *State Key Laboratory of Photocatalysis on Energy and Environment, College of Chemistry, Fuzhou University, Fuzhou 350002, China*
[c] *PIMM, Arts et Metiers ParisTech, CNRS, Cnam, HESAM Université, 151 Blvd. de L'Hôpital, Paris 75013, France*
[d] *Department of Nuclear Science and Engineering, Massachusetts Institute of Technology (MIT), Cambridge, MA 02139, USA*
[e] *State Key Laboratory of Powder Metallurgy, Central South University, Changsha 410083, China*

A B S T R A C T

This paper reports a new liquid metal embrittlement (LME) system in which a dual-phase $Al_{0.7}CoCrFeNi$ (equimolar fraction) high-entropy alloy (HEA) is embrittled by lead-bismuth eutectic (LBE) at 350 and 500°C. At 350°C, (Ni, Al)-rich BCC phase is embrittled, leading to intragrain cracking within this phase, while the predominant cracking mode changes to BCC/FCC phase boundary decohesion at 500°C. At both temperatures, cracks are rarely seen in the (Co, Cr, Fe)-rich FCC phase, indicating that this phase is immune to LME. Furthermore, the results suggest a transition from an adsorption-dominated LME mechanism at 350°C to a phase boundary wetting-dominated LME mechanism at 500°C.

Liquid lead-bismuth eutectic ($Pb_{44.5}Bi_{55.5}$, wt%, LBE) is an important working fluid for Gen IV fast reactors and accelerator driven transmutation systems (ADS), due to its beneficial thermo-hydraulic and neutronic properties as well as inherent safety [1]. Nevertheless, the deployment of this technology is technically impeded by incompatibility issues of steels when exposed to LBE, including the so-called liquid metal embrittlement (LME) and liquid metal corrosion (LMC) [1,2]. LME in presence of LBE occurs mainly in ferritic/martensitic steels (F/M, e.g., T91, HT9, and EP823) at around 350°C, leading to severe deterioration of ductility and toughness of these steels when stressed in contact with this liquid metal [3–8]. LMC can occur in the F/M steels and austenitic stainless steels (AuSS, e.g., 316L and 15-15Ti), manifested by either surface oxidation when LBE is rich in oxygen or by selective leaching of the steel elements (e.g., Ni, Mn, Cr, and Fe) when oxygen in LBE is poor [9]. In particular, the locally-enhanced dissolution, known as "pitting", represents the most undesired corrosion mode and poses a serious threat to thin-walled components, such as fuel cladding and heat exchanger tubes [10–15]. These issues can jeopardize the safe operation of the reactors.

Corresponding authors.
E-mail addresses: gongxing@szu.edu.cn (X. Gong), yuzyemlab@gmail.com (Z. Yu).

To better take the advantage of LBE-cooled fast reactors, it is necessary to explore new materials with higher resistance to the harsh LBE environment at elevated temperatures. In recent years, high-entropy alloys (HEAs) have received increasing research interests for their unique microstructures and appealing properties [16–19]. Unlike traditional alloys that contain only a couple of major elements, HEAs consist of at least roughly five equimolar principal elements, leading to a series of interesting characteristics, such as a maximum configurational entropy of the whole alloy system stabilizing solid solutions, sluggish diffusion, and strong lattice distortion, etc. A large number of studies have demonstrated that HEAs possess excellent mechanical properties [16–18], high corrosion and stress corrosion cracking resistance [20–22], as well as good irradiation resistance [23,24]. Among them, the $Al_xCoCrFeNi$ type is one of the most investigated HEAs [16,25–28].

In this paper, an $Al_{0.7}CoCrFeNi$ (at.%) HEA was selected for the LME study, considering that this alloy is a dual-phase structure (FCC + BCC) that benefits to a relatively good balance of strength and ductility [25]. In addition, this alloy contains 14.89 at.% (i.e., about 7.73 wt.%) Al, and thus can form a passivating and protective alumina scale that is very important for corrosion resistance as reported in Ref. [29]. The phase diagrams with lead or bismuth of most of the constituents of the alloy (Al, Fe, Cr, Co) show an immiscibility gap in the solid state with limited high temperature sol-

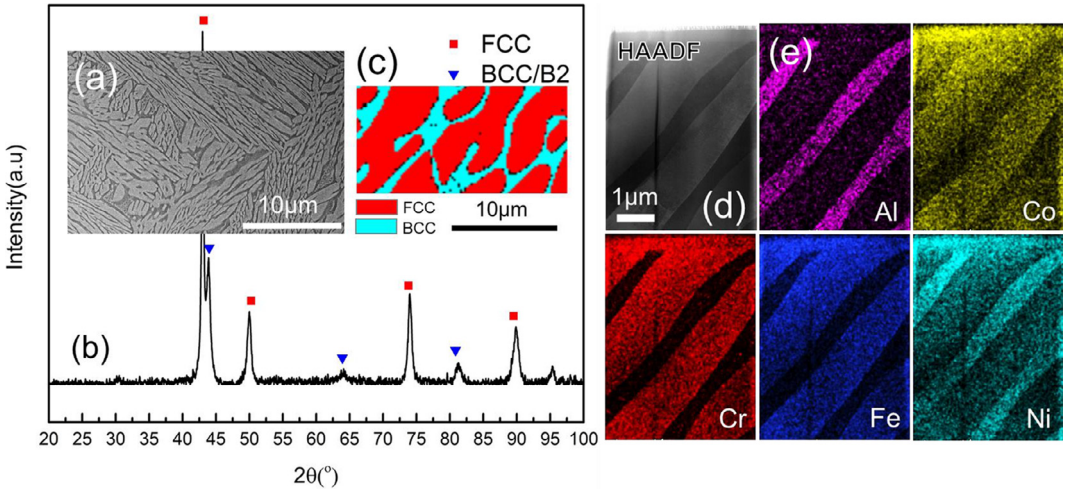

Fig. 1. SEM micrograph (a), XRD pattern (b), EBSD phase map (c), HAADF image (d) and EDS maps (e) of the as-received dual-phase $Al_{0.7}CoCrFeNi$ high-entropy alloy. Note: the BCC phase and FCC phase are identified by EBDS using the standard PDF cards of BCC-structured NiAl and FCC-structured austenite, respectively (c).

ubility [30]. Only the Ni/Bi system shows some intermetallic compounds. In most cases, the immiscibility between the solid and the liquid phase is a good indicator for a possible LME behavior. Therefore, a few screening tensile tests were performed to assess the LME susceptibility of this alloy in contact with LBE at 350 and 500°C. The results show that this alloy is susceptible to LME, manifested by a significant reduction in total elongation to rupture. To the best of our knowledge, this is a new LME system that was not reported in the past. The underlying LME mechanism of this system is discussed, based on multiscale microstructural characterizations.

The $Al_{0.7}CoCrFeNi$ alloy was fabricated by vacuum induction melting at 1700°C. The obtained cast ingots were then manufactured into cylindrical tensile specimens with a gauge length of 15 mm and a gauge diameter of 3 mm. The specimens were tested in oxygen-saturated LBE at 350 and 500°C using our test facility "LABET-1" [31]. The saturated oxygen concentrations at these two temperatures were estimated to be 3.4×10^{-5} wt% and 8.08×10^{-4} wt%, respectively, according to the equation [32]. $logC_{o,s}(wt.\%) = 2.62 - \frac{4416}{T(K)}$. Before starting the tests, the specimens were pre-exposed to oxygen-saturated LBE at 500°C for about 20 h. Reference tests were performed in air at the same temperatures. All tests were carried out under a nominal strain rate of 5×10^{-5} s^{-1}.

The original microstructure of the $Al_{0.7}CoCrFeNi$ alloy was examined by scanning electron microscope (SEM, Thermofisher Scientific Scios), X-ray diffraction (XRD, Miniflex600), electron backscatter diffraction (EBSD, Oxford, NordlysMax), and transmission electron microscopy (TEM, Thermofisher Scientific Talos F200s). After the tensile testing in LBE, the fractured specimen was cleaned in a chemical solution composed of CH_3COOH (acetic acid), CH_3CH_2OH (ethanol) and H_2O_2 (hydrogen peroxide) with a volume ratio of 1:1:1 for SEM fractographic examinations. Focused ion beam (FIB, Thermofisher Scientific Helios600i) was used to prepare site-specific lamellas at crack tips for TEM examinations.

SEM micrograph, XRD pattern and EBSD phase identification map in Fig. 1a–c show that the $Al_{0.7}CoCrFeNi$ alloy is composed of a dendritic FCC phase and an interdendritic BCC/B2 phase. High-angle annular dark field (HAADF) image and EDS maps in Fig. 1d and e reveal that the FCC phase is rich in Co, Cr and Fe with a thickness of 1~5 μm, while Al and Ni are the major constitutive elements of the BCC phase and this phase mostly has a thickness ranging from several hundred nanometers to 1 μm. These results are in good agreement with those reported by Wang et al. [25,26].

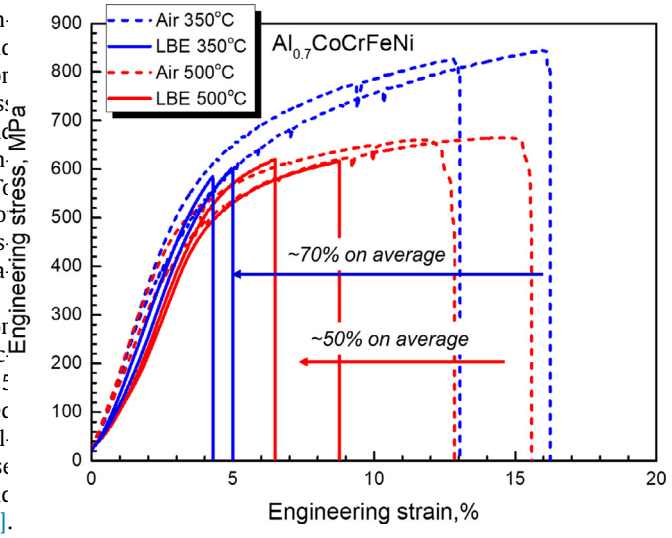

Fig. 2. Engineering tensile stress-strain curves of the dual-phase $Al_{0.7}CoCrFeNi$ high-entropy alloy tested in oxygen-saturated LBE and air at 350 and 500°C (the curves are not corrected with the compliance of the mechanical testing machines).

Fig. 2 presents the engineering tensile stress-strain curves of the $Al_{0.7}CoCrFeNi$ alloy tested in oxygen-saturated LBE and air at 350 and 500°C. It can be seen that this alloy shows high strength and acceptable ductility when tested in air at both temperatures (see the dashed lines). When tested in LBE, yield strength is not altered, but strong ductility loss occurs in comparison to that in air. This is a typical sign of LME. The ductility loss is more severe at 350°C (by ~70%) than that at 500°C (by ~50%), which results from the improved ductility when the test temperature is raised. Moreover, the occurrence of LME also suggests that this Al-enriched alloy cannot form sufficiently protective and robust oxide scales in the presence of the oxygen-saturated LBE to prevent LME.

Fig. 3 examines the fracture surfaces and longitudinal cross-sections of the specimens tested in air and LBE at 350 and 500°C, showing large differences. For the specimen tested in air at 350°C (Fig. 3a), the fracture surface shows a mixture of cleavage of the (Ni, Al)-rich BCC phase and tearing of the (Co, Cr, Fe)-rich FCC phase. This implies that the (Ni, Al)-rich BCC phase is already brittle at 350°C, while the (Co, Cr, Fe)-rich FCC phase may have some ductility. This is to be expected, since nickel aluminides in-

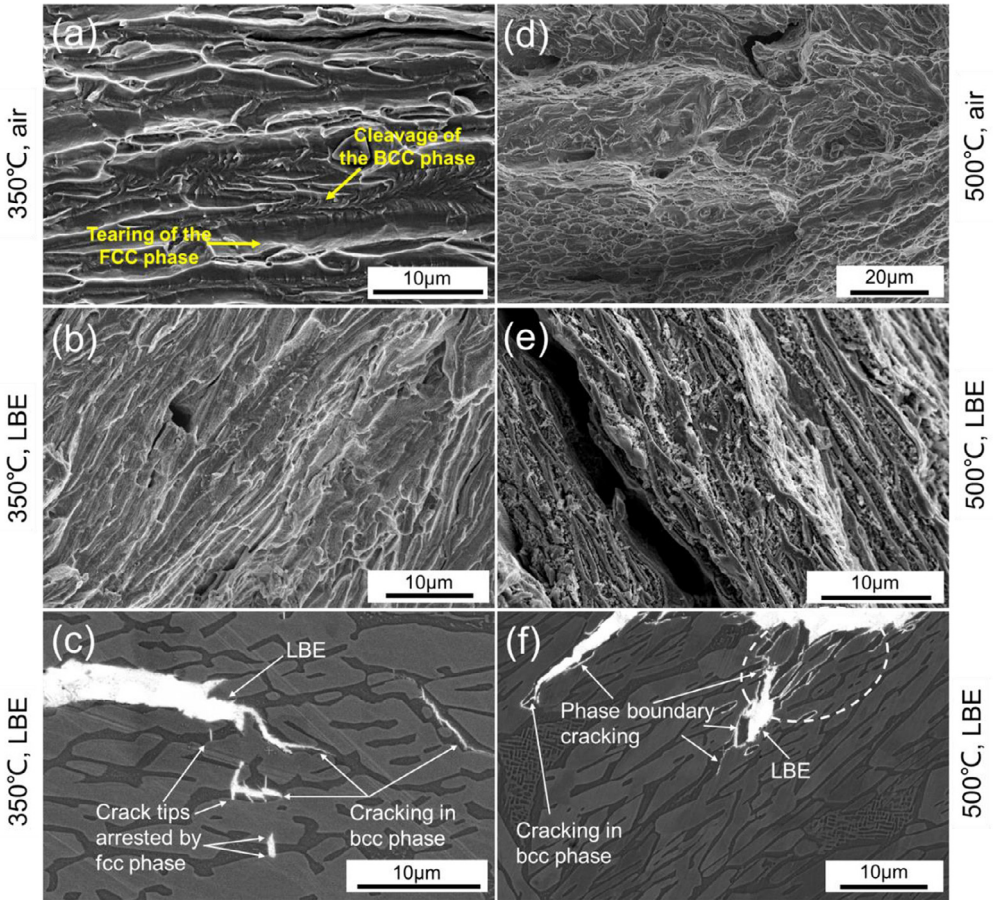

Fig. 3. SEM micrographs of the fracture surfaces (a, b, d and e) and longitudinal cross-sections (c and f) of the dual-phase $Al_{0.7}CoCrFeNi$ high-entropy alloy after testing in LBE and air at 350 and 500°C.

termetallics are known to be brittle at low temperatures [33]. For the specimen tested at the same temperature but in LBE (Fig. 3b), the fracture surface does not exhibit evident differences in comparison to that in air (Fig. 3a), but fiber-like surface patterns start to stand out. The SEM backscatter micrograph of the longitudinal cross-section reveals more clearly the cracking paths (Fig. 3c). It can be seen from this figure that the cracks are filled completely with LBE up to the crack tips, suggesting good wetting of LBE on the crack walls. The cracks propagate mainly inside the (Ni, Al)-rich BCC phase, with only a small part going along the BCC/FCC phase boundaries. One may notice that the (Co, Cr, Fe)-rich FCC phase can arrest the crack tips (see the arrows in Fig. 3c). This observation indicates that the FCC phase is not susceptible to LME. The LME insensitivity of this phase is similar to that of another FCC-structured HEA ($Fe_{40}Mn_{10}Ni_{10}Co_{20}Cr_{20}$, at.%) reported in our previous work [31]. Therefore, the severe ductility loss at 350°C (Fig. 2) must be attributed to the premature cracking of the (Ni, Al)-rich BCC phase and this phase is susceptible to LME. Increasing the test temperature from 350 to 500°C improves the ductility of the alloy in air, since cleavage of the BCC phase is less frequent than that at 350°C and ductile dimpling is visible locally (Fig. 3d). The fracture surface of the specimen tested in LBE at 500°C is much different from that tested in air at the same temperature (Fig. 3e). It can be seen that massive fiber-like structures are seen on the fracture surface. The formation of this fiber-like pattern is a result of decohesion of BCC/FCC phase boundaries, as shown in Fig. 3f. It is clearly shown from this figure that the density of the locations where LBE penetrates into the BCC/FCC phase boundaries as a thin intergranular film is remarkably increased (see the arrows and dashed circle) compared to that at 350°C (Fig. 3c), though a few cracks propagating inside the BCC phase are still visible. These results suggest that the LME mechanism of this alloy at 500°C is most likely linked to phase boundary wetting with intergranular penetration of LBE (with eventually a diffusive step).

The HAADF image in Fig. 4a shows that a crack in the specimen tested in LBE at 350°C propagates inside the BCC phase that in fact is a single grain. The high-resolution TEM (HRTEM) images in Fig. 4b and c further reveal that the cracking planes change alternately from the main plane $(\bar{2}\bar{1}1)$ to the secondary plane $(\bar{2}00)$, and finally this crack is arrested at the $(02\bar{2})$ and (064) planes of the FCC phase. Increasing the test temperature to 500°C mainly leads to the decohesion of the BCC/FCC phase boundaries and a small amount of BCC phase cracking (Fig. 5a). At this relatively high temperature, the main cracking plane in the BCC phase falls into the same crystallographic plane family as that at 350°C, i.e., $(\bar{2}1\bar{1})$, while the secondary cracking plane changes to $(01\bar{1})$, as shown in Fig. 5b. In the case of the phase boundary decohesion (Fig. 5c and d), LBE penetrates preferentially into the phase boundaries with the planes of $(\bar{2}1\bar{1})$ and $(01\bar{1})$ at the BCC phase side and with the planes of $(11\bar{1})$ and (200) at the FCC phase side, forming a very thin LBE film with a thickness of about 28 nm (Fig. 5c). Both specimens tested at 350 and 500°C do not show formation of new phases along the cracking paths or at the crack tips in accordance with the immiscibility of the relevant binary phase diagrams.

LME systems can be categorized into two groups. One group is linked to grain boundary wetting phenomenology, in which the energetics that drives a liquid metal into grain boundaries of a solid metal is the difference between the grain boundary energy (γ_{gb})

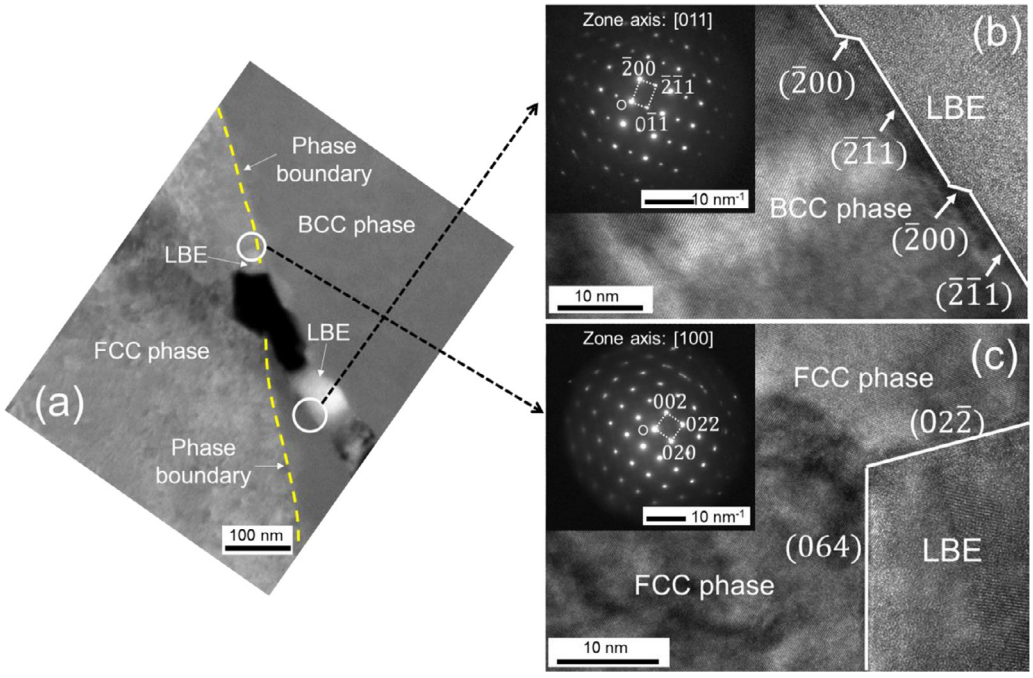

Fig. 4. A HAADF image (a) and two HRTEM images (b and c) showing that the crack propagates inside the BCC phase and along certain low index planes, and finally is arrested at the FCC phase. The TEM lamellae was extracted from a specimen tested in oxygen-saturated LBE at 350°C.

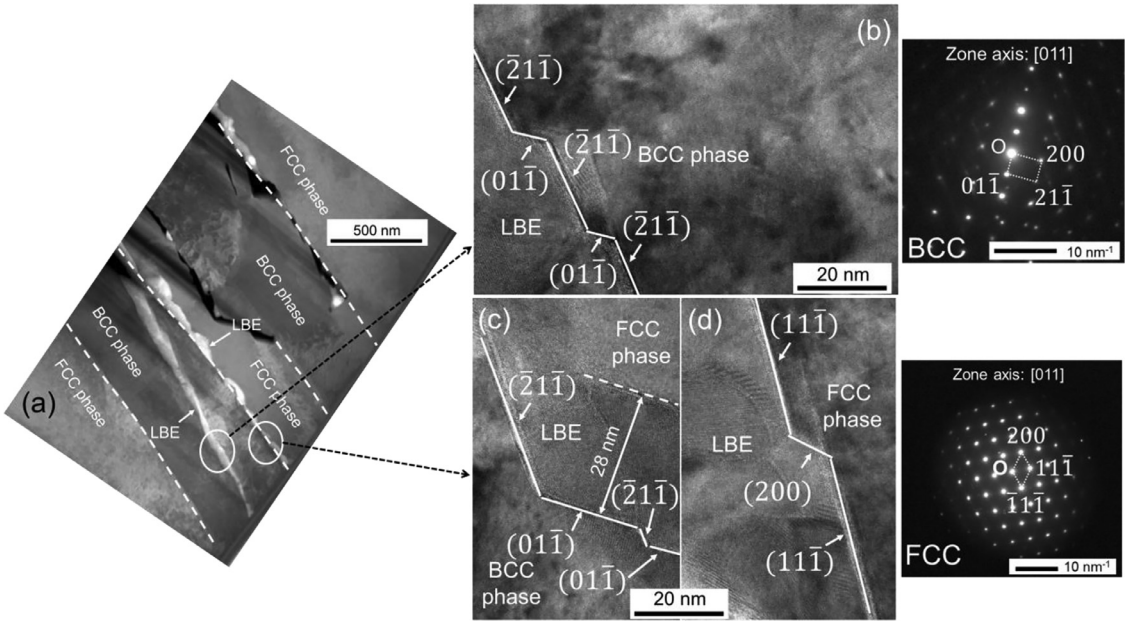

Fig. 5. A HAADF image (a) and three HRTEM images (b, c and d) showing that cracks propagate mainly along the BCC/FCC phase boundaries, with a few intragrain cracking cases within the BCC phase. The TEM lamellae was extracted from a specimen tested in oxygen-saturated LBE at 500°C.

and the interfacial energies of the solid metal/liquid metal contacting interfaces ($2\gamma_{sl}$). In this group, beyond a wetting temperature, $2\gamma_{sl} < \gamma_{gb}$, then liquid metal can spontaneously enter the grain boundaries of the solid metal without applied stress and the dihedral angle drops to zero. Those systems, including Al/Ga [34], Cu/Bi [35,36], Ni/Bi [37,38], Mo/Ni [39], etc., are typical cases of this group. The other group needs external factors, e.g., stress, to aid the liquid metal to attack the grain boundaries or bulk of the solid metal, such as the T91/LBE and FeCrAl/LBE systems [40,41]. In this case, various models have been proposed to describe the LME mechanisms, including adsorption induced reduction in surface energy [42], adsorption induced reduction in interatomic cohesion [43,44], adsorption enhanced dislocation emission [45,46], stress assisted dissolution/condensation [47,48], and grain boundary diffusion under stress [49,50], etc. Among them, the most widely accepted ones are the adsorption induced reduction in surface energy or interatomic cohesion models.

For the present $Al_{0.7}CoCrFeNi$/LBE system, the fracture mechanism at 350°C is most likely governed by adsorption of LBE atoms at crack tips and subsequent weakening of the atomic bonds of the alloy, because of the following two arguments: First, the cracks propagate mainly in a transgranular way in the BCC phase without evident penetration of LBE into the grain and interphase boundaries (Figs. 3c and 4); Second, the cracking planes contain the (100)

and (112) plane families with clear cut facets that seem immune to localized dissolution (the most soluble element Ni has a solubility limit of only 1.2~1.5% at 350~400° C according to the equation: $logC_s$ (wppm) $= 5.53 - \frac{843}{T}$, $673K < T < 1173K$ [9]). Therefore, stress assisted dissolution/condensation and grain boundary diffusion mechanisms do not account for the observed LME phenomenon at 350°C. Note that the BCC phase is already very brittle at 350°C as expected (Fig. 3a). This means that LBE makes this phase even more brittle due to the remarkable ductility loss (Fig. 2).

When the test temperature increases to 500°C, the ductility of the BCC phase improves (Fig. 3d). NiAl intermetallic has a very high ductile-brittle transition temperature (DBTT, ~1000°C) [33], but the BCC phase may not be a pure NiAl phase (Fig. 1e) and the small amount of Co may have significantly lowered down its DBTT. This ductility recovery may partly account for the observed lower frequency of cracking inside the BCC phase at 500°C than at 350°C. On the other hand, the significantly increased number of the BCC/FCC phase boundary cracking at 500°C (Fig. 3e and f) indicates that a phase boundary wetting transition of LBE is enhanced. Such a strong temperature dependence of grain boundary wettability exists in several other solid metal/liquid metal systems, such as Fe or Fe-based alloys/LBE system. For instance, grain boundary wetting is not widely observed in an Fe-based Fe10Cr4Al alloy when mechanically tested at 350°C [41], while a stronger tendency of grain boundary grooving and wetting occurs at the grain boundaries of pure α-Fe without the aid of mechanical stress, when the exposure temperature is increased to 900°C [51]. Thus, this is a new LME system involving phase boundary wetting at high temperature, in addition to the aforementioned ones. This phase boundary wetting mechanism is somewhat different from the steel/Zn system in which grain boundary wetting is accompanied by formation of new intermetallic phases and occurrence of phase transformation [52]. In our case, new phases are not detected by HRTEM (Figs. 4 and 5), but ordered bi-dimensional structures at atomic scale cannot be excluded as similar to what is observed in the Ni/Bi system [37,38]. More interestingly, the phase boundary wetting transition must be enhanced by the tensile stresses that can open the interatomic space in the vicinity of the liquid metal penetration front, because the stress-free corrosion test result presented in Fig. S1 shows that a maximum LBE penetration depth of 257 μm was formed after exposure for 500 h, corresponding to a penetration rate of only 0.514 μm/h, while the LME-induced sudden stress drop in Fig. 2 occurs in less than one second, corresponding to a cracking rate of as high as ~3000 μm/s (the specimen diameter is 3 mm and the sudden stress drop takes place prior to necking). Since the LME cracking rate is huge, the pure diffusion-controlled creep mechanisms such as Coble creep may not play a predominant role in this fast rupture process, especially when LME also occurs at 350°C that is not a typically high temperature for creep. More likely, the liquid metal follows the fast propagating crack tips by capillarity and the crack tips move preferentially along those phase boundaries that are normal to the maximum tensile stress and are wetted by LBE. This leads to a strong tendency of forming a flat fracture surface (Fig. S2). In addition, the LME cracking follows mostly the low index crystallographic planes (Figs. 4 and 5), where the lowest energy criterion should apply.

It is also worth noting that the cracks that propagate in the BCC phase and along the BCC/FCC phase boundaries are microscopically not very straight (Figs. 4 and 5). This may be attributed to local fluctuations in defects, chemical composition and microstructure of the $Al_{0.7}$CoCrFeNi alloy. For instance, Figs. S3 and S4 show that there are numerous nanosized Cr-rich precipitates locating in the BCC phase and at the BCC/FCC phase boundaries after the mechanical testing, and these precipitates are probably some kind of Cr-rich intermetallics as similar to what was reported in Ref. [26]. These fluctuations can impact somehow the wetting behavior of LBE and the crack propagation paths at microscopical scale. Furthermore, HEAs should be treated as a "whole-solute matrix" and a "defective reference state", meaning that averaged atomic size and classical wetting do not exist and the LME phenomenon in this study may involve some atomic-scale mechanisms that deviate from those of the classical grain boundary wetting cases. However, this issue is beyond the scope of this article and future work is needed for a clearer answer.

In summary, this paper reports a new LME system. It is found that the dual-phase (FCC + BCC) $Al_{0.7}$CoCrFeNi (equimolar fraction) high-entropy alloy is embrittled by LBE at 350 and 500°C. The LME characteristics are temperature-dependent. At 350°C, cracks propagate mainly within the (Ni, Al)-rich BCC phase and along certain low-index planes, indicating that the BCC phase is susceptible to LME. At 500°C, cracking at the BCC/FCC phase boundaries is the predominant failure mode. This temperature dependence of the LME cracking behaviors suggests a transition from an adsorption-dominated LME mechanism at 350°C to a phase boundary wetting-controlled LME mechanism at 500°C. At both temperatures, cracks are rarely observed in the FCC phase, implying that this phase is immune to LME. This LME case with an intermetallic phase has some parallels with the case of beta-brass LME in the ordered B2 (CsCl type) composition range as well [53]. Given the strong LME susceptibility, this HEA material is not recommended for use in LBE environment.

Declaration of Competing Interest

The authors declare that they have no known competing financial interests or personal relationships that could have appeared to influence the work reported in this paper.

Acknowledgment

This work is financially supported by National Natural Science Foundation of China (Grant No. 51801129 and 51701170) and Natural Science Foundation of Shenzhen University, China (Grant no. 85304-00000302) .

Supplementary materials

Supplementary material associated with this article can be found, in the online version, at doi:10.1016/j.scriptamat.2020.113652.

References

[1] OECD/NEA, Handbook on lead-bismuth eutectic alloy and lead properties, materials compatibility, thermal-hydraulics and technologies, 2015.
[2] X. Gong, R. Li, M.Z. Sun, Q.S. Ren, T. Liu, M.P. Short, J. Nucl. Mater. 482 (2016) 218–228.
[3] D. Gorse, T. Auger, J.-B. Vogt, I. Serre, A. Weisenburger, A. Gessi, P. Agostini, C. Fazio, A. Hojná, F. Di Gabriele, J. Nucl. Mater. 415 (2011) 284–292.
[4] E. Stergar, S.G. Eremin, S. Gavrilov, M. Lambrecht, O. Makarov, V. Lakovlev, J. Nucl. Mater. 473 (2016) 28–34.
[5] X. Gong, P. Marmy, Y. Yin, J. Nucl. Mater. 509 (2018) 401–407.
[6] F. Ersoy, S. Gavrilov, K. Verbeken, J Nucl. Mater. 472 (2016) 171–177.
[7] A. Hojná, P. Halodová, M. Chocholoušek, Z Špirit, L. Rozumová, Corros. Rev. 38 (2020) 183–194.
[8] I. Proriol Serre, J.-B. Vogt, J. Nucl. Mater. 531 (2020) 152021.
[9] J.S. Zhang, N. Li, J. Nucl. Mater. 373 (2008) 351–377.
[10] V. Tsisar, C. Schroer, O. Wedemeyer, A. Skrypnik, J. Konys, J. Nucl. Mater. 454 (2014) 332–342.
[11] V. Tsisar, C. Schroer, O. Wedemeyer, A. Skrypnik, J. Konys, J. Nucl. Mater. 468 (2016) 305–312.
[12] K. Lambrinou, E. Charalampopoulou, T. Van der Donck, R. Delville, D. Schryvers, J. Nucl. Mater. 490 (2017) 9–27.
[13] K. Lambrinou, V. Koch, G. Coen, J. Van den Bosch, C. Schroer, J. Nucl. Mater. 450 (2014) 244–255.

[14] V. Tsisar, C. Schroer, O. Wedemeyer, A. Skrypnik, J. Konys, J. Nucl. Eng. Radiat. Sci. 5 (2019) 031201.
[15] C. Schroer, V. Tsisar, A. Durand, O. Wedemeyer, A. Skrypnik, J. Konys, J Nucl. Eng. Radiat. Sci. 5 (2019) 011006.
[16] E.P. George, W.A. Curtin, C.C. Tasan, Acta Mater. 188 (2020) 435–474.
[17] Z.Z. Li, S.T. Zhao, R.O. Ritchie, M.A. Meyers, Prog. Mater. Sci. 102 (2019) 296–345.
[18] P. Sathiyamoorthi, H.S. Kim, Prog. Mater. Sci. (2020) In press https://doi.org/10.1016/j.pmatsci.2020.100709 .
[19] K. Biswas, J.-W. Yeh, P.P. Bhattacharjee, J.T.M. De Hosson, Scr. Mater. 188 (2020) 54–58.
[20] Y.Z. Shi, L. Collins, R. Feng, C. Zhang, N. Balke, P.K. Liaw, B. Yang, Corros. Sci. 133 (2018) 120–131.
[21] H. Luo, W.J. Lu, X.F. Fang, D. Ponge, Z.M. Li, D. Raabe, Mater. Today 21 (2018) 1003–1009.
[22] Y.K. Zhao, D.H. Lee, M.Y. Seok, J.A. Lee, M.P. Phaniraj, J.Y. Suh, H.Y. Ha, J.Y. Kim, U. Ramamurty, J. Jang, Scr. Mater. 135 (2017) 54–58.
[23] K. Jin, C. Lu, L.M. Wang, J. Qu, W.J. Weber, Y. Zhang, H. Bei, Scr. Mater. 119 (2016) 65–70.
[24] T.F. Yang, W. Guo, J.D. Poplawsky, D.Y. Li, L. Wang, Y. Li, W.Y. Hu, M.L. Crespillo, Z.F. Yan, Y. Zhang, Y.G. Wang, S.J. Zinkle, Acta Mater. 188 (2020) 1–15.
[25] W.R. Wang, W.L. Wang, S.C. Wang, Y.C. Tsai, C.H. Lai, J.W. Yeh, Intermetallics 26 (2012) 44–51.
[26] J.C. Rao, H.Y. Diao, V. Ocelík, D. Vainchtein, C. Zhang, C. Kuo, Z. Tang, W. Guo, J.D. Poplawsky, Y. Zhou, P.K. Liaw, J.T.M. De Hosson, Acta Mater. 131 (2017) 206–220.
[27] I. Basu, V. Ocelík, J.T.M. De Hosson, Acta Mater. 150 (2018) 104–116.
[28] I. Basu, J.T.M. De Hosson, Scr. Mater. 187 (2020) 148–156.
[29] J. Lu, Y. Chen, H. Zhang, L. Li, L.M. Fu, X.F. Zhao, F.W. Guo, P. Xiao, Corros. Sci. 170 (2020) 108691.
[30] Phase Equilibria, Crystallographic and Thermodynamic Data of Binary Alloys. Landolt-Börnstein - Group IV Physical Chemistry. Vol. 5. Springer.
[31] X. Huang, X. Gong, M. Song, J.J. Chen, F.Y. Hu, Y. Yin, J. Xiao, H. Wang, H. Wang, H.R. Gong, Y.B. Deng, B. Pang, Y.C. Li, J. Nucl. Mater. 528 (2020) 151859.
[32] C. Schroer, J. Konys, Physical Chemistry of Corrosion and Oxygen Control in Liquid Lead and Lead-Bismuth Eutectic, Report No. FZKA 7364, Karlsruhe, Germany.
[33] A. Lasalmonie, Intermetallics 14 (2006) 1123–1129.
[34] E. Pereiro-Lopez, W. Ludwig, D. Bellet, P. Cloetens, C. Lemaignan, Phys. Rev. Lett. 95 (2005) 215501.
[35] A. Kundu, K.M. Asl, J. Luo, M.P. Harmer, Scr. Mater. 68 (2013) 146–149.
[36] G. Duscher, M.F. Chisholm, U. Alber, M. Rühle, Nat. Mater. 3 (2004) 621–626.
[37] J. Luo, H. Cheng, K.M. Asl, C.J. Kiely, M.P. Harmer, Science 333 (2011) 1730–1733.
[38] Z.Y. Yu, P.R. Cantwell, Q. Gao, D. Yin, Y.Y. Zhang, N.X. Zhou, G.S. Rohrer, M. Widom, J. Luo, M.P. Harmer, Science 358 (2017) 97–101.
[39] X.M. Shi, J. Luo, Appl. Phys. Lett. 94 (2009) 251908.
[40] X. Gong, P. Marmy, A. Volodin, B. Amin-Ahmadi, L. Qin, D. Schryvers, S. Gavrilov, E. Stergar, B. Verlinden, M. Wevers, Corros. Sci. 102 (2016) 137–152.
[41] X. Gong, J.J. Chen, F.Y. Hu, C.Y. Xiang, Z.Y. Yu, J. Xiao, H. Wang, H.R. Gong, H. Wang, C.H. Liu, Y.B. Deng, B. Pang, X. Huang, Y.C. Li, Y. Yin, Corros. Sci. 165 (2020) 108364.
[42] W. Rostoker, J.M. McCaughey, H. Markus, Embrittlement of Liquid Metals, Reinhold Publishing Corporation, New York, 1960.
[43] N.S. Stoloff, T.L. Johnston, Acta Metall. 11 (1963) 251–256.
[44] A.R.C. Westwood, M.H. Kamdar, Philos. Mag. 8 (1963) 787–804.
[45] S.P. Lynch, Acta Metall. 29 (1981) 325–340.
[46] S.P. Lynch, Metall. Mater. Trans. A 44 (2013) 1209–1229.
[47] W.M. Robertson, Trans. Metall. Soc. AIME 236 (1966) 1478–1482.
[48] E.E. Glickman, Metall. Mater. Trans. A 42 (2011) 250–266.
[49] C. Hancock, M.B. Ives, Can. Metall. Q. 10 (1971) 207–211.
[50] P. Gordon, H.H. An, Metall. Trans. A 13 (1982) 457–472.
[51] S.Q. Ma, J.S. Zhang, Mater. Charact. 147 (2019) 43–49.
[52] L. Cho, H. Kang, C. Lee, B.C. De Cooman, Scr. Mater. 90 (2014) 25–28.
[53] M.M. Shea, N.S. Stoloff, Mater. Sci. Eng. 12 (1973) 245–253.